Cutis laxa, exocrine pancreatic insufficiency and altered cellular metabolomics as additional symptoms in a new patient with ATP6AP1-CDG

Bianca Dimitrov, Nastassja Himmelreich, Agnes L. Hipgrave Ederveen, Christian Lüchtenborg, Jürgen G. Okun, Maximilian Breuer, Anna-Marlen Hutter, Matthias Carl, Luca Guglielmi, Andrea Hellwig, Kai Christian Thiemann, Markus Jost, Verena Peters, Christian Staufner, Georg F. Hoffmann, Annette Hackenberg, Nagarajan Paramasivam, Stefan Wiemann, Roland Eils, Matthias Schlesner, Sabine Strahl, Britta Brügger, Manfred Wuhrer, G. Christoph Korenke, Christian Thiel

Cutis laxa, exocrine pancreatic insufficiency and altered cellular metabolomics as additional symptoms in a new patient with ATP6AP1-CDG

Bianca Dimitrov[a,1], Nastassja Himmelreich[a,1], Agnes L. Hipgrave Ederveen[b],
Christian Lüchtenborg[c], Jürgen G. Okun[a], Maximilian Breuer[a], Anna-Marlen Hutter[a],
Matthias Carl[d,n], Luca Guglielmi[d,n], Andrea Hellwig[e], Kai Christian Thiemann[a], Markus Jost[a],
Verena Peters[a], Christian Staufner[a], Georg F. Hoffmann[a], Annette Hackenberg[f],
Nagarajan Paramasivam[g,h,o], Stefan Wiemann[i,j], Roland Eils[h,k,o], Matthias Schlesner[h,o],
Sabine Strahl[l], Britta Brügger[c], Manfred Wuhrer[b], G. Christoph Korenke[m], Christian Thiel[a,*]

[a] *Center for Child and Adolescent Medicine, Department I, Im Neuenheimer Feld 669, 69120 Heidelberg, Germany*
[b] *Leiden University Medical Center, Center for Proteomics and Metabolomics, Albinusdreef 2, 2333 ZA Leiden, Netherlands*
[c] *Heidelberg University Biochemistry Center (BZH), Im Neuenheimer Feld 328, 69120 Heidelberg, Germany*
[d] *Department of Cell and Molecular Biology, Medical Faculty Mannheim, Heidelberg University, 68167 Mannheim, Germany*
[e] *Department of Neurobiology, Interdisciplinary Center for Neurosciences, Heidelberg University, Im Neuenheimer Feld 364, 69120 Heidelberg, Germany*
[f] *Division of Pediatric Neurology, University Children's Hospital Zürich, Steinwiesstrasse 75, 8032 Zürich, Switzerland*
[g] *Medical Faculty Heidelberg, Heidelberg University, 69120 Heidelberg, Germany*
[h] *Division of Theoretical Bioinformatics, German Cancer Research Center (DKFZ), Im Neuenheimer Feld 280, 69120 Heidelberg, Germany*
[i] *Genomics & Proteomics Core Facility, German Cancer Research Center (DKFZ), Im Neuenheimer Feld 580, 69120 Heidelberg, Germany*
[j] *Division of Molecular Genome Analysis, German Cancer Research Center (DKFZ), Im Neuenheimer Feld 580, 69120 Heidelberg, Germany*
[k] *Department for Bioinformatics and Functional Genomics, Institute for Pharmacy and Molecular Biotechnology (IPMB), BioQuant, Heidelberg University, 69120 Heidelberg, Germany*
[l] *Centre for Organismal Studies (COS), Glycobiology, Heidelberg University, Im Neuenheimer Feld 360, 69120 Heidelberg, Germany*
[m] *Klinikum Oldenburg, Zentrum für Kinder-und Jugendmedizin, Klinik für Neuropädiatrie u. angeborene Stoffwechselerkrankungen, Rahel-Straus-Straße 10, 26133 Oldenburg, Germany*
[n] *Laboratory of Translational Neurogenetics, Center for Integrative Biology, University of Trento, 39123 Trento, Italy*
[o] *Bioinformatics and Omics Data Analytics (B240), German Cancer Research Center (DKFZ), Im Neuenheimer Feld 280, 69120 Heidelberg, Germany*

ABSTRACT

Congenital disorders of glycosylation (CDG) are genetic defects in the glycoconjugate biosynthesis. > 100 types of CDG are known, most of them cause multi-organ diseases. Here we describe a boy whose leading symptoms comprise cutis laxa, pancreatic insufficiency and hepatosplenomegaly. Whole exome sequencing identified the novel hemizygous mutation c.542 T > G (p.L181R) in the X-linked ATP6AP1, an accessory protein of the mammalian vacuolar H^+-ATPase, which led to a general N-glycosylation deficiency. Studies of serum *N*-glycans revealed reduction of complex sialylated and appearance of truncated diantennary structures. Proliferation of the patient's fibroblasts was significantly reduced and doubling time prolonged. Additionally, there were alterations in the fibroblasts' amino acid levels and the acylcarnitine composition. Especially, short-chain species were reduced, whereas several medium- to long-chain acylcarnitines (C14-OH to C18) were elevated. Investigation of the main lipid classes revealed that total cholesterol was significantly enriched in the patient's fibroblasts at the expense of phophatidylcholine and phosphatidylethanolamine. Within the minor lipid species, hexosylceramide was reduced, while its immediate precursor ceramide was increased. Since catalase activity and ACOX3 expression in peroxisomes were reduced, we assume an ATP6AP1-dependent impact on the β-oxidation of fatty acids. These results help to understand the complex clinical characteristics of this new patient.

---

1. Introduction

The maintenance of pH homeostasis is essential for almost all cellular processes in an organism as structure, function and solubility of numerous proteins depend on a particular pH-value [1,2]. A variety of regulatory mechanisms control the pH, e.g. direct proton transport, indirect proton coupling to other ion transports or vacuolar H^+-AT-Pases (V-type H^+-ATPase, V-ATPase). The 1000 kDa V-ATPase is a multi-subunit complex which belongs to the family of V0V1-ATP synthases [3].

It is organized in the membranous V0 and the cytosolic V1 domain [4,5]. In mammals the V0 domain consists of nine subunits (a1, a2, a3, a4, d1, d2, c, c″ and e) while the V1 domain is composed of 13 subunits (A, B1, B2, C1, C2, D, E1, E2, F, G1, G2, G3 and H) [3]. Also accessory proteins are involved. The V-ATPase complex uses a V1-mediated and ATP-hydrolyzing rotor mechanism to transport protons across the cell membrane which then enter the V0 domain through a cytoplasmic hemichannel.

In recent years, a number of defects have been identified in different subunits of the V-ATPase in humans, as e.g. infantile malignant autosomal recessive osteopetrosis caused by mutations in *ATP6V0A3* (V0 subunit a3, also named TCIRG1) or the autosomal recessive renal tubular acidosis due to mutations in *ATP6V1B1* or *ATP6V0A4*, respectively [6,7,8,9]. Furthermore, mutations in the accessory subunit '(Pro)renin receptor' (M8-9 encoded by *ATP6AP2*) result in X-linked intellectual disability, epilepsy and parkinsonism [10,11]. Moreover, several defects of V-ATPase subunits influence the protein glycosylation machinery leading to distinct subtypes within the group of rare and heterogeneous metabolic diseases, called Congenital Disorders of Glycosylation (CDG) [12]. Deficiency of the V0 subunit α2 leads to ATP6V0A2-CDG [13], whereas ATP6V1A-CDG and ATP6V1E1-CDG are defects of the V1 subunits A and E1 [7]. These defects belong to CDG-II that affect the structure of N- and often also mucin-type O-glycans. In 2016 eleven male CDG-II patients with hemizygous mutations in the V-ATPase accessory subunit AC45 (ATP6AP1) were identified. The patients show mainly immunodeficiency (including hypogammaglobulinemia), hepatopathy and a spectrum of neurocognitive abnormalities [14].

Here we describe an ATP6AP1-CDG patient with a new hemizygous mutation and additional features such as rapidly improving cutis laxa, exocrine pancreatic insufficiency, treatable diarrhea as well as changes in the amino acid and lipid metabolism.

2. Material and methods

2.1. Patient material

The study was performed in accordance with the Declaration of Helsinki and approved by the Ethics Committee of the Medical Faculty Heidelberg. Written informed consent was obtained from the parents of the patient for whole-exome sequencing. The parents also consented to molecular testing (Sanger sequencing) of their own ATP6AP1-status. Written informed consent was also obtained for use of photographs and clinical information.

2.2. Isoelectric focusing of serum transferrin

IEF of serum transferrin was performed as described by Niehues et al. [15].

2.3. Isoelectric focusing of apolipoprotein-CIII

IEF of ApoCIII was performed as described by Wopereis et al. [16].

2.4. Western blotting

Western blotting was performed as described by Lübbehusen et al. [17]. An HRP-coupled secondary antibody in a dilution of 1:10,000 in PBST was used for 1 h at RT. Visualization was performed by adding a chemiluminescence reagent (Pierce). Primary antibodies against ATP6AP1 (Sigma-Aldrich, rabbit anti-human, 1:500), HiF1α (Thermo-Fisher, mouse anti-human, 1:1000), ACOX3 (Atlas Antibodies, rabbit anti-human, 1:1000), BiP (Cell Signaling, rabbit anti-human, 1:1000) and LC3 (Novusbio, rabbit anti-human, 1:500) were used. Secondary antibodies used for Western blots were horseradish peroxidase (HRP)-conjugates (Dianova, goat anti-rabbit; Santa Cruz, goat anti-mouse).

2.5. Glycan analysis

N-glycans derived from patient and control fibroblasts were analyzed as described by Reiding et al. [18].

2.6. Whole exome sequencing (WES)

Trio-based WES (Agilent SureSelect target enrichment and Illumina HiSeq 2000 paired end sequencing) and analysis of the sequence data were performed at the German Cancer Research Center (DKFZ) at Heidelberg (Germany) using the previously described Heidelberg exome data analysis bioinformatics pipeline. Variants with a minor allele frequency (MAF) > 1% in the Exome Aggregation Consortium (ExAC) and 1000 genome phase III database were considered common alleles and removed from the candidate list. Local control samples were used to remove the recurrent technical artifacts and common alleles that were not seen in the above databases. Only non-synonymous exonic variants and variants ± 2 bases around the intron-exon junction, classified as splice-site variants, nonsense variants and indels were further considered [19]. Variants were assessed by 7 different variant effect prediction tools (SIFT, PolyPhen2, LRT, MutationTaster, MutationAssessor, FATHMM, and PROVEAN) from dbNSFP v2.0 and CADD scores. Sequence validation of the detected mutation was performed on cDNA and exon level by using Sanger sequencing (see below). The mutation was uploaded to ClinVar Submission Wizard (SUB2942359; www.ncbi.nlm.nih.gov/clinvar/).

2.7. Reverse transcriptase PCR

Using random hexamer primers (Invitrogen) and Maxima™ Reverse Transcriptase (Thermo Fisher) 500 ng of total RNA were reverse transcribed into cDNA. PCR was performed with 50 ng of cDNA as template using *ATP6AP1* specific primers *ATP6AP1*-Fw (5′-CCCAGTACATGACC TTATGGG-3′) and *ATP6AP1*-Rev (5′-GGTTAGTTCAAATAAGGCA CAG-3′) with *Pfu*-Turbo-Polymerase (Stratagene).

2.8. Quantitative real-time PCR

Quantitative real-time PCR was carried out by SensiFAST SYBR No-ROX-Mix (Bioline) with 50 ng of reverse transcribed RNA in a CFX Connect Real-Time System (BioRad) with the following parameters: step 1: 95 °C, 2 min; step 2: 95 °C, 15 s; step 3: 60 °C, 10 s; step 4: 72 °C, 10 s; step 5: 100 °C to 25 °C, 5 min; step 6: 4 °C, forever. Steps 2–4 were repeated 35-times. Primers used were ATP6AP1-qPCR-Fw (5′-GAGTG ACCGGGACTTGTGG-3′), *ATP6AP1*-qPCR-Rev (5′-CAGGAAGCACCAGT GAGGAG-3′), *RAB7A*-qPCR-Fw (5′-TGGGAGATTCTGGAGTCGGG-3′) and *RAB7A*-qPCR-Rev (5′-CACACCGAGAGACTGGAACC-3′). Expression levels were normalized to *Ras-related protein* (*RAB7A*).

2.9. Sanger sequencing

ATP6AP1-cDNA (RefSeq NM_001183.5) was analyzed on a 1% agarose gel and extracted with the QIAquick gel extraction kit (Qiagen).

Sequence analysis was performed by dye-terminator cycle sequencing with primers *ATP6AP1*-Fw and *ATP6AP1*-Rev. Exon 4 of genomic DNA from control and patient fibroblasts (QIAamp DNA Mini Kit, Qiagen) was amplified with primers *ATP6AP1*-Ex4-Fw1 (5′-GAGCAGAGACGCT GGCTTTG-3′), *ATP6AP1*-Ex4-Rev1 (5′-GCTCAGTGCTAGGCACC AAC-3′) and *ATP6AP1*-Ex4-Fw2 (5′-GCCTTTATGGGTATGGCTTGC-3′), *ATP6AP1*-Ex4-Rev2 (5′-GGAGTACTGGCATCTTTAGCC-3′) from 100 ng template using *Pfu*-Turbo-Polymerase (Stratagene). After preincubation at 95 °C for 1 min followed by 30 cycles with 1 min at 94 °C, 0.5 min at 55 °C and 1 min at 68 °C, PCR products were extracted from a 1.5% agarose gel and sequenced with the secondary primers.

2.10. Cell lines and cell culture

Fibroblasts from the patient and controls were cultivated at 37 °C under 5% CO_2 in DMEM-high glucose (PAA) containing 10% FCS (PAN Biotech GmbH) and 100 U/ml Penicillin/Streptomycin (PAA).

2.11. Cell proliferation studies by live cell monitoring

Cell proliferation was assessed by following the manufacturer's guidelines using the XCelligence device (ACEA Biosciences). We seeded 1000 cells to the measuring cavities culturing them under standard conditions for 120 h. Cell density was computer-based recorded every 30 min. Quantification was carried out with slope values (1/h) measured during the logarithmic growth phase.

2.12. Immunofluorescence

One day before preparation, 5×10^4 fibroblasts were seeded on glass cover slips. Immunofluorescence was carried out as described [20]. Cells were stained with antibodies against ATP6AP1 (Sigma-Aldrich, rabbit anti-human, 1:300) and GM130 (BD Transduction Laboratories, mouse anti-human, 1:500) or ERGIC-53 (Enzo Life Sciences, mouse anti-human, 1:500). After incubation with fluorochrome-conjugated secondary antibodies, Alexa Fluor 488 (ThermoFisher, goat anti-rabbit, 1:500) or Alexa Fluor 568 (ThermoFisher, goat anti-mouse, 1:500), cells were mounted with Mowiol and analyzed by confocal fluorescence microscopy.

2.13. Amino acid and acylcarnitine analyses

Amino acid and acylcarnitine contents of patient and control fibroblast homogenates (100 µg) were analyzed as described by Okun et al. [21].

2.14. Electron microscopy

Fibroblasts were fixed, dehydrated and embedded. Resin ultrathin sections were examined using a ZEISS transmission electron microscope [22].

2.15. Lipid analysis

Quantitative lipid analysis was performed with 100 µg from control and patient fibroblasts according to Özbalci, Sachsenheimer and Brügger [23].

2.16. Lipid oil analysis

The detection of neutral lipids within cultured cells was carried out with the Lipid (Oil Red O) staining kit (Abnova). One day before preparation, 5×10^4 cells were seeded on a 24 well plate. The cell staining was assessed according to the manufacturer's guidelines.

2.17. Determination of catalase activity

0.5×10^6 fibroblasts in the logarithmic growth phase were used for the assay. Further procedure was conducted with the catalase activity assay kit (Abcam).

2.18. Statistics

All experiments were repeated at least three times. Data were analyzed using the Student's *t*-test for single comparisons or one-way ANOVA followed by Bonferroni's test for multiple comparisons. Significances of p-values: * ≤ 0.05; ** ≤ 0.005; *** ≤ 0.001. Data are displayed as mean ± SD.

3. Results

3.1. Clinical characteristics

The family history is unremarkable regarding metabolic and neurological disorders. Abnormalities during pregnancy comprised pathological nuchal fold, mild intrauterine tricuspid insufficiency and arachnoid cyst. The patient was born in the 39th week of pregnancy with a birth weight of 3270 g (40th percentile), length of 50 cm (25th percentile) and head circumference of 35.5 cm (70th percentile). Directly after birth a remarkable cutis laxa predominantly at the abdomen, arms and legs (Fig. 1, A) was observed. In the 3rd month of life the patient was diagnosed with splenomegaly and in the 6th month it was found that the small fontanelle was bigger than the large fontanelle. A turricephalus, high forehead, small interocular distance, pseudostrabismus, exocrine pancreatic insufficiency (trypsin < 2.5 µg/l, ref. val. 10.0–57.0 µg/l; pancreas elastase < 15.0 µg/g, ref. val. > 200.0 µg/g) and joint hypermobility of fingers, elbows and knees were observed, as well. Further symptoms included muscular hypotonia and hepatomegaly (midclavicular length 8 cm) with hepatopathy without cholestasis. In relation to this, investigations showed elevated AST (110 U/l, ref. val. < 40 U/l) and ALT (69 U/l, ref. val. < 45 U/l). The patient also presented with developmental disability, failure to thrive, diarrhea and glomerular and tubular dysfunction. He began to speak, slightly delayed, with the age of 1 ½ years. The severe diarrhea due to pancreatic insufficiency was successfully treated with Kreon (25,000 U/day) and the decreased blood fat-soluble vitamins A, D, E and K were substituted. Additionally, hematological abnormalities comprised normocytic anemia (hemoglobin 8.7 g/dl, hematocrit 24.1%), thrombocytopenia (83,000/µl) and coagulant dysfunction (e.g. PTT 60.3 s, ref. val. < 37 s; ATIII 38%, ref. val. 80–120%; fibrinogen 1.3 g/dl, ref. val. 1.8–3.5 g/dl). Laboratory investigations showed elevated total cholesterol (207 mg/dl, ref. val. < 170 mg/dl) as well as reduced copper (5.5 µmol/l, ref. val. 12.6–19.0 µmol/l) getting along with reduced ceruloplasmin (0.15 g/l, ref. val. 0.2–0.6 g/l). Recurrent infections and reduced amounts of antibodies after vaccinations (e.g. measles, mumps, rubella, varicella) pointed towards immunodeficiency and laboratory results revealed reduced immunoglobulin (IgG 474.0 mg/dI, ref. val. 572.0–1474 mg/dI; IgA 14 mg/dI, ref. val. 34–305 mg/dI). Psychomotor development was grossly normal. At the age of 5 he learned to bike and swim. He joined a regular preschool till the age of 6 and then changed to elementary school. Furthermore the spleen was enlarged (120 mm × 40 mm) but showed a normal echographic pattern. The accessory spleen which had already been noticed at age 6 with a diameter of 1.5 cm × 1.8 cm had a size of around 16 mm. No signs of ascites were found. At age 8 8/12 his height was 135.7 cm (between 50th–75th percentile) with a body weight of 27.8 kg (50th percentile). The right liver lobe was enlarged (77 mm × 110 mm) and showed two hyperechogenic alterations in segment II and segment V, without signs of cirrhosis. Electrocardiography, electroencephalography and motoric nerve conduction velocity (tibial nerve) were normal. His skin looked fair with sheer veins and mild cutis laxa still persisting around the
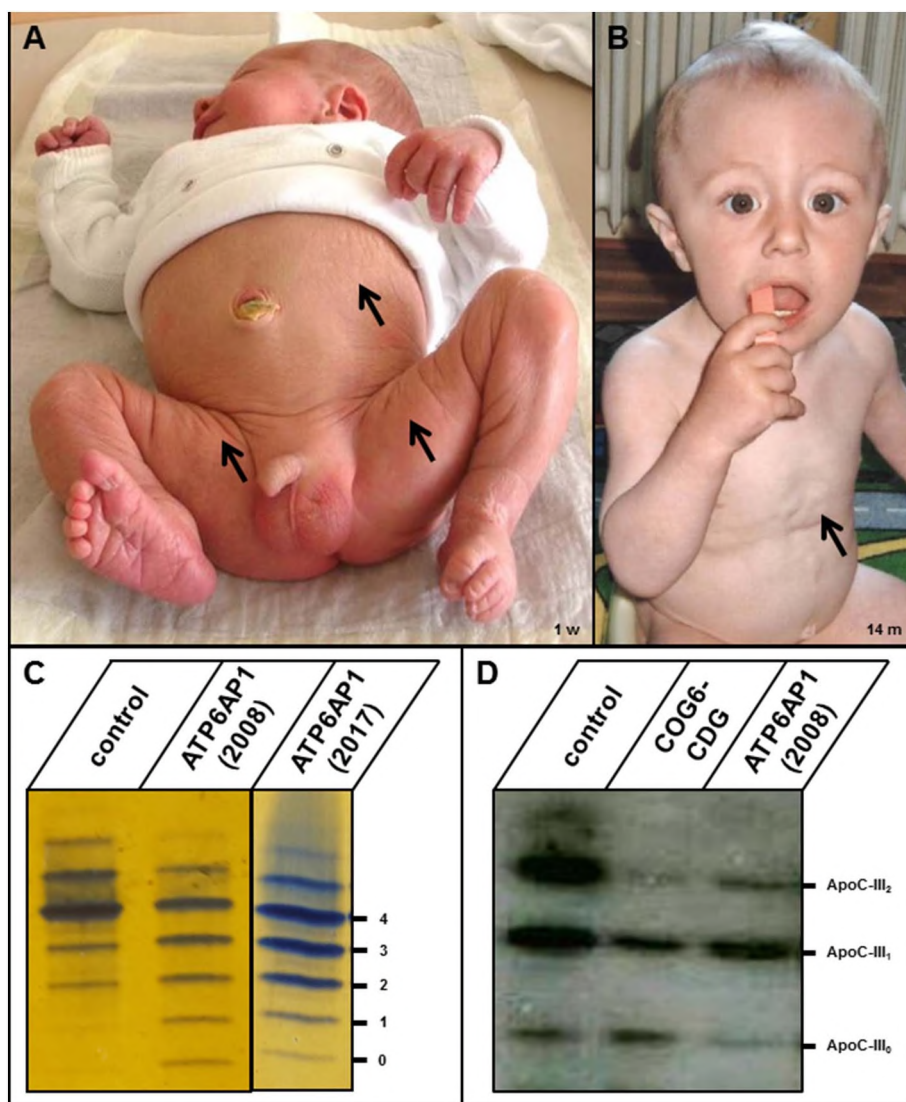
Fig. 1. Symptoms of cutis laxa and confirmation of an N-glycosylation deficiency by serum transferrin IEF of patient and control samples. (A) Patient at one week of age with cutis laxa most noticeable around the thighs and the abdomen (arrows). (B) Consecutive improvement of cutis laxa with patient growth. Residual wrinkly skin between chest and abdomen at the age of 14 months (arrows). (C) Serum samples of a control (lane 1) and the patient (lanes 2–3) were investigated by serum transferrin IEF. Numbers 0 to 4 indicate asialo-, monosialo-, disialo-, trisialo- and tetra-sialotransferrin, respectively. Please note that the serum sample used in lane 2 was from the year of birth (2008) and that of lane 3 was taken in 2017 showing a mild improvement of hypoglycosylation. Quantification of transferrin isoforms can be found in the text. (D) Core-1 mucin-type O-linked glycans of ApoCIII of a healthy control (lane 1), a CDG-II positive control (COG6-CDG, lane 2) and the ATP6AP1-CDG patient (lane 3) were investigated by IEF. $ApoCIII_2$, $ApoCIII_1$ and $ApoCIII_0$ indicate the amount of sialic acid residues linked to ApoCIII.
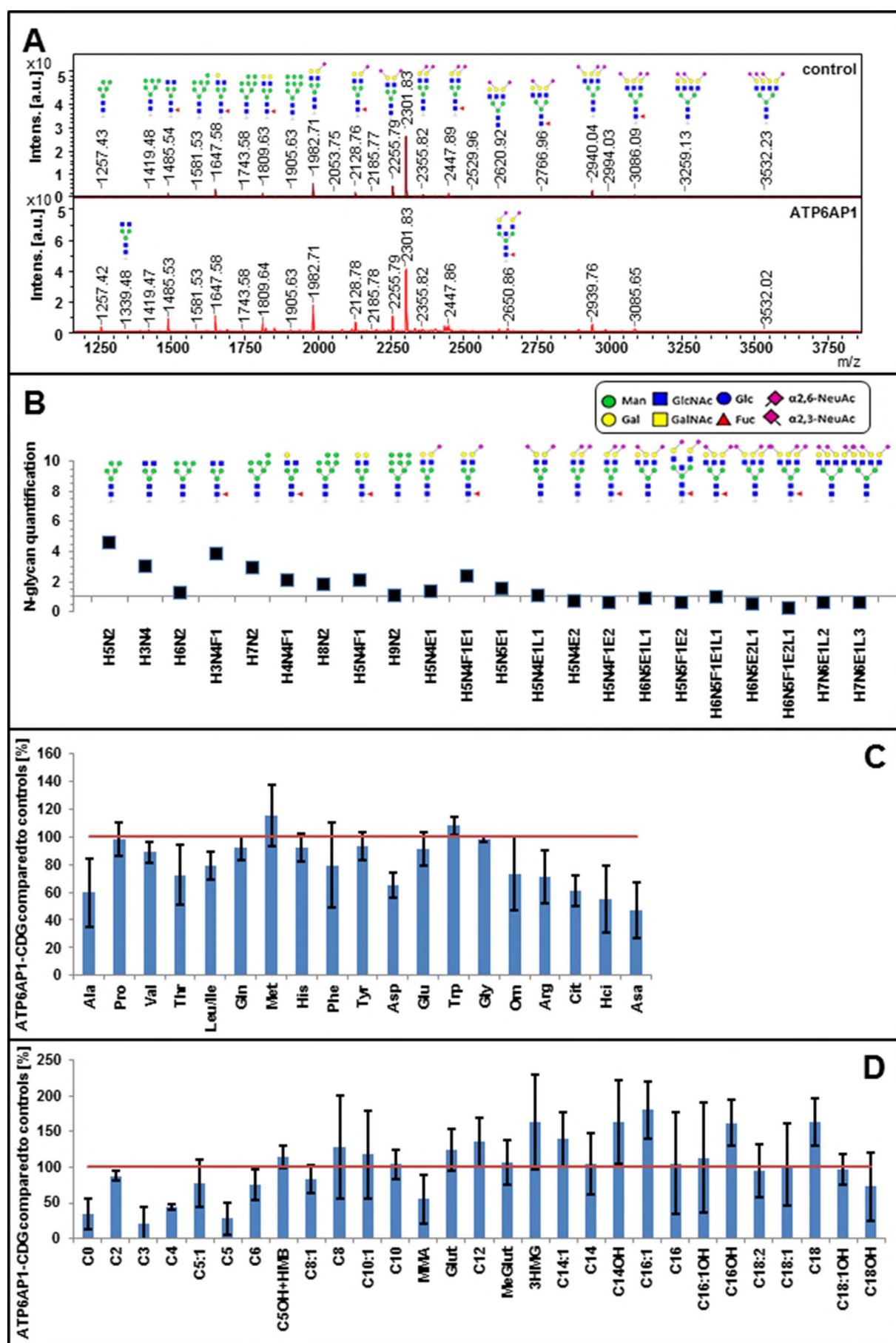
abdomen. Nevertheless, cutis laxa improved significantly over time at arms and legs, and persisted mainly in a milder form around the abdomen (Fig. 1, B). Blood coagulation normalized. Meanwhile (2018) he is visiting a regular high school.

3.2. Hypoglycosylation of serum transferrin but control-like apolipoprotein-CIII pattern

The patient was tested for CDG by isoelectric focusing (IEF) of serum transferrin (Fig. 1, C). In 2008 a CDG type II pattern was found: tetrasialotransferrin 28.4%, ref. val. 30.0%–55.0%; trisialotransferrin 21.3%, ref. val. 4.0%–17.5%; disialotransferrin 14.7%, ref. val. 5.0%-13.5%; monosialotransferrin 7.9%, ref. val. 0.0%–3.0% and asialo-transferrin 6.1%, ref. val. 0.0%–2.0%. In 2017 the quantity of tetra-sialo-(38.4%) and asialotransferrin (1.6%) reached normal values. Trisialo-(31.3%) and disialotransferrin (21.3%) were slightly more pronounced, whereas monosialotransferrin (7.3%) was slightly diminished. An IEF of serum apolipoprotein-CIII (ApoCIII; Fig. 1, D) to investigate core 1 mucin type O-glycans revealed normal values for the three different ApoCIII isoforms ($ApoCIII_2$ 45.3%, ref. val. 27.4%–60.0%; $ApoCIII_1$ 38.7%, ref. val. 33.1%–66.9%; $ApoCIII_0$ 15.9%, ref. val. 0.0%–11.6%).

3.3. N-glycan analysis revealed reduction of complex sialylated and emergence of truncated diantennary structures

Serum glycans were measured on reflectron positive MALDI-TOF-MS after sialic acid stabilization (Fig. 2, A). In contrast to the controls (n = 6; age-matched) our patient (serum from 2008) showed increased truncated diantennary structures (Fig. 2, B). Aside from the most prominent peak for $Man_5GlcNAc_2$ (H5N2, m/z 1257.42; H = hexose, N = N-acetylhexosamine) which presented with a 4.6 times higher value, the core fucosylated truncated (i.e. non-galactosylated) diantennary glycan (H3N4F1, m/z 1485.54, 3.78-fold higher; F = fucose) and the not fucosylated $GlcNAc_2Man_3GlcNAc_2$ glycan (H3N4, m/z 1339.48, 2.96-fold higher) as well as $Man_7GlcNAc_2$ species (H7N2, m/z 1743.58, 2.94-fold elevated) were considerably elevated. In parallel, we detected a general reduction of complex sialylated structures from H5N4E2 (m/z 2355.82; E = 2,6-linked N-acetylneuraminic acid) to H7N6E1L3 (m/z 3532.23; L = 2,3-linked N-acetylneuraminic acid) with values ranging from 0.93 for H6N5F1E1L1 (m/z 2766.96) to 0.26 for H6N5F1E2L1 (m/z 3086.09). Next to the shorter complex-type sugar moieties the overall distribution of N-glycans in the ATP6AP1-CDG patient revealed a shift from complex type to more mannose-rich and hybrid type glycans in comparison to controls. While in controls the ratio between complex type, mannose-rich and hybrid type N-glycans was about 96.6% ± 0.6% to 2.1% ± 0.4% to 0.7% ± 0.2%, in the
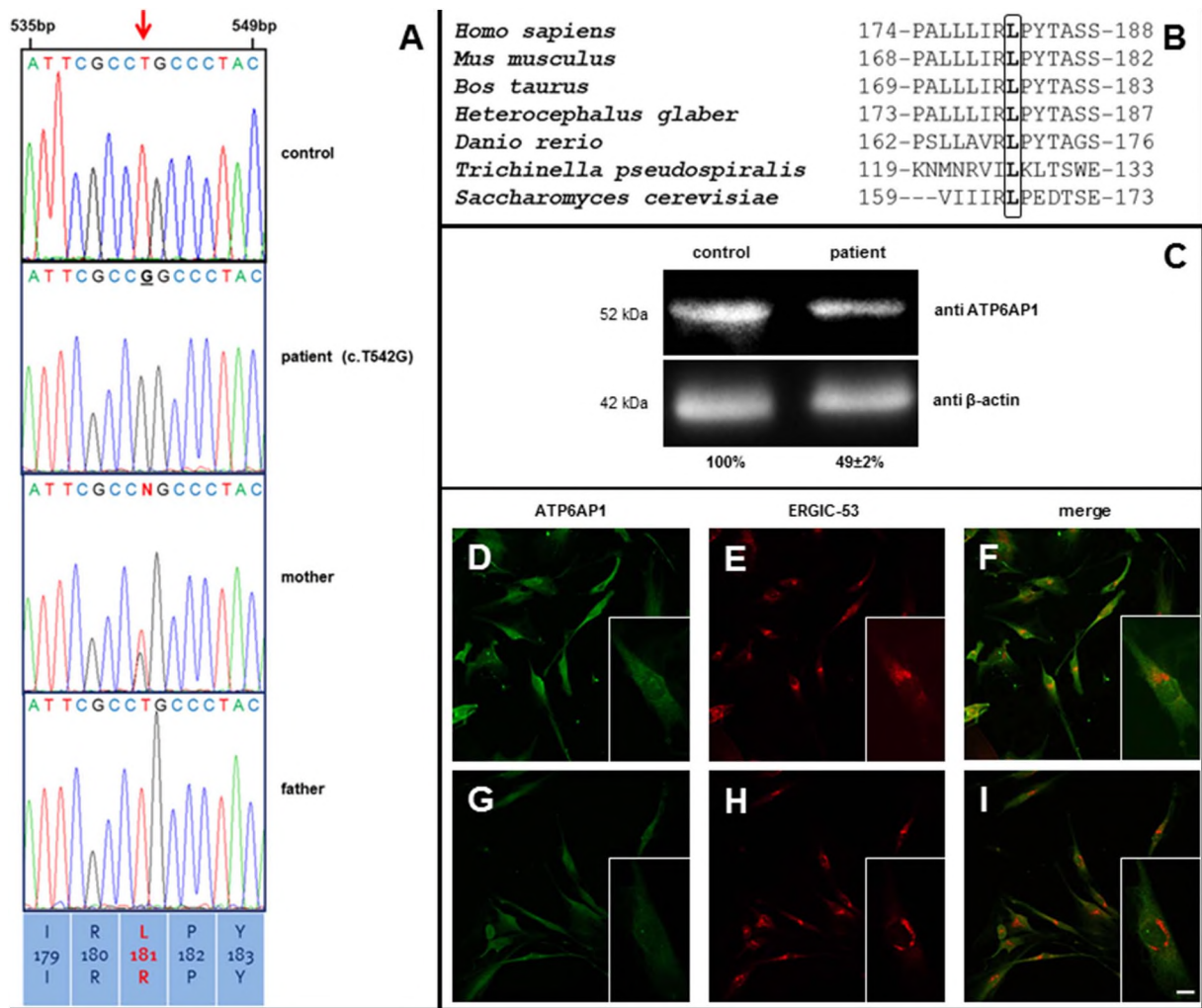
(caption on next page)

Fig. 3. Characterization of the mutated ATP6AP1 on DNA, protein and cellular level. (A) Sanger sequencing confirms the hemizygous mutation c.542 T > G in exon 4 of the patient's *ATP6AP1* gene on the X-chromosome. The father is unaffected whereas the mother is the heterozygous carrier. (B) The ATP6AP1 mutation p.L181R affects a highly conserved amino acid within species. (C) Quantification of patient's ATP6AP1 by Western blot analysis revealed a reduction in comparison to controls. (D-I) Immunofluorescence studies in patient-derived fibroblasts showed a reduced signal for ATP6AP1 in comparison to the control, but a control-like co-localization with ERGIC-53. Magnification 63 ×, bar: 10 μm.

patient values of 94.2% to 4.0% to 1.2% were measured. Although the complex types (minus of 3%) were not significant, a significant plus of 93% for the mannose-rich and 80% for the hybrid structures was detected (Suppl. Table 1).

3.4. Whole exome sequencing identified a mutation in the ATP6AP1 gene

Whole exome sequencing showed the new hemizygous mutation c.542 T > G in exon 4 of the X-linked (Xq28) *ATP6AP1* gene. This was confirmed by Sanger sequencing (Fig. 3, A). The patient's father is unaffected while the mother is the heterozygous carrier of the mutation leading to the amino acid exchange p.L181R. As leucin 181 is located in a highly conserved stretch of ATP6AP1 (NP_0011774.2) across species (Fig. 3, B), a significant role of this amino acid for the protein's function is assumed.

3.5. Reduced amount of ATP6AP1 protein due to mRNA depletion but normal protein localization in the cell

On Western blot analysis, ATP6AP1 of the patient was reduced to 48.9% ± 1.9% (Fig. 3, C). As this could either be due to instability of the mutated protein or the patient's *ATP6AP1* mRNA, qRT-PCR studies were initiated which revealed that the quantity of the patient's *ATP6AP1* mRNA was reduced to 57% ± 1%. Immunofluorescence studies further showed that the mutated protein is located in a control-like manner in the cell characterized by co-localization of ATP6AP1 with ERGIC-53 (Fig. 3, D–I), though presenting with a weakened fluorescent signal. No co-staining of ATP6AP1 with GM130 was seen (data not shown).

3.6. Retarded cell growth with prolonged doubling and reduced proliferation time

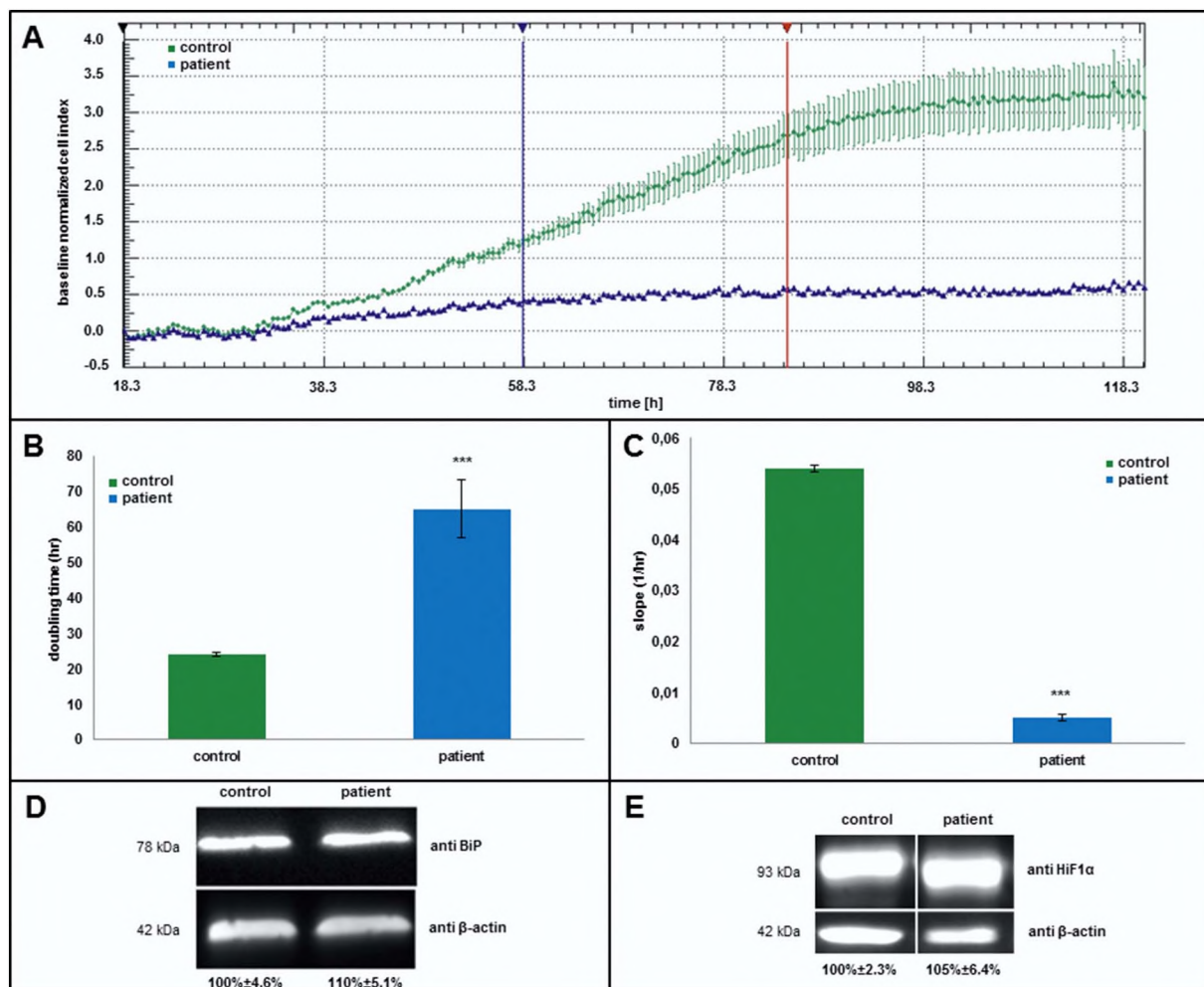As the patient's fibroblasts grew much slower than control cell lines,

Fig. 4. Analysis of cell growth. (A) XCelligence device analysis of cell proliferation of a control (green) and the patient (blue) measured over 5 days. (B) ATP6AP1-deficient cells needed about three times longer for doubling compared to control fibroblasts and showed a significantly reduced cell proliferation (C). (D) Western Blot analysis of BiP (HSP70, normalized to β-actin) in the patient's fibroblasts detected a slightly elevated but significant difference between control and patient, whereby the expression of HiF1α was not affected in the patient (E).

we measured the cells' doubling time and proliferation. Comparison of the slope values measured during the logarithmic growth phase (between ~58 h to 84 h; Fig. 4, A) showed that the patient's fibroblasts needed 2.7 times longer (65.2 h ± 8.1 h; controls 24.2 h ± 0.5 h; Fig. 4, B). Besides, the proliferation of the patient's fibroblasts was severely reduced to 9.4% ± 1.1% in contrast to the control (Fig. 4, C). To investigate whether ER stress or hypoxia-mediated apoptosis was causal, we determined the level of BiP and HiF1-α by Western blotting and found a small but significant upregulation of BiP (110.4% ± 5.1%, *p ≤ 0.028; Fig. 4, D), whereas HiF1-α remained control-like (105.9% ± 6,4%; Fig. 4, E). Morphological investigations by electron microscopy could not reveal consistent abnormalities in the patient fibroblasts (data not shown).

3.7. ATP6AP1 deficiency impacts the amino acid and acylcarnitine composition in fibroblasts

Next we investigated if the ATP6AP1 deficiency influences the amino acid and acylcarnitine composition, as well as cellular lipid homeostasis. Tandem mass spectrometry analysis of homogenates derived from patient and control fibroblasts (set to 100%) showed that the patient's amino acid levels were at borderline or even reduced (Fig. 2, C) with alanine (59.6% ± 24.7%), threonine (72.2% ± 21.6%), aspartic acid (65.1% ± 9.1%), ornithine (73.2% ± 26.6%), arginine (71.3% ± 19.3%), citrullin (60.9% ± 11.1%), homocitrulline (54.9% ± 24.3%) and argininosuccinate (47.1% ± 20.0%) as lowest-

rated metabolites. Acylcarnitine analysis showed an overall reduction of short-chain as well as accumulation of several medium- to long-chain acylcarnitines in the patient fibroblasts (Fig. 2, D). Regarding the short-chain metabolites, carnitine (C0, 3.0-fold), propionylcarnitine (C3, 4.7-fold), butyrylcarnitin (C4, 2.3-fold) and isovalerylcarnitine (C5, 3.6-fold) were strongly reduced, whereas 3-hydroxyisovalerylcarnitine + β-hydroxymethylbutyrate (C5OH + HMB, 1.1-fold) and the medium-chain acylcarnitines octanoylcarnitine (C8, 1.3-fold), decenoylcarnitine (C10:1, 1.2-fold) and decanoylcarnitine (C10, 1.0-fold) were increased. Most notably, several long-chain acylcarnitines were elevated, predominantly 3-hydroxy-3-methylglutaric- (3HMG, 1.6-fold), tetradecenoyl- (C14:1, 1.4-fold), 3-hydroxytetradecenoyl- (C14OH, 1.6-fold), hexadecenoyl- (C16:1, 1.8-fold), hydroxyhexadecanoyl- (C16OH, 1.6-fold) and octadecanoylcarnitine (C18, 1.6-fold). Only octadeca-dienoyl- (C18:2, 1.0-fold), hydroxyoctadecenoyl- (C18:1OH, 1.0-fold) and hydroxyoctadecanoylcarnitine (C18OH, 1.4-fold) were diminished. Interestingly, a significant increase of the saturated, very long-chain, branched phytanic 1498% ± 37,3% (***p ≤ 0.00002) and pristanic acid 870% ± 30% (***p ≤ 0.0008) was detected.

3.8. ATP6AP1 depletion affects the lipid homeostasis

CuSO₄-treated fibroblasts stained with Oil Red O showed an elevated signal intensity in patient cells (189.2% ± 46.6%, ***p ≤ 0.0002; controls 100% ± 15.5%; Fig. 5, A, B and C), suggesting an impairment of lipid homeostasis. Mass spectrometry analysis
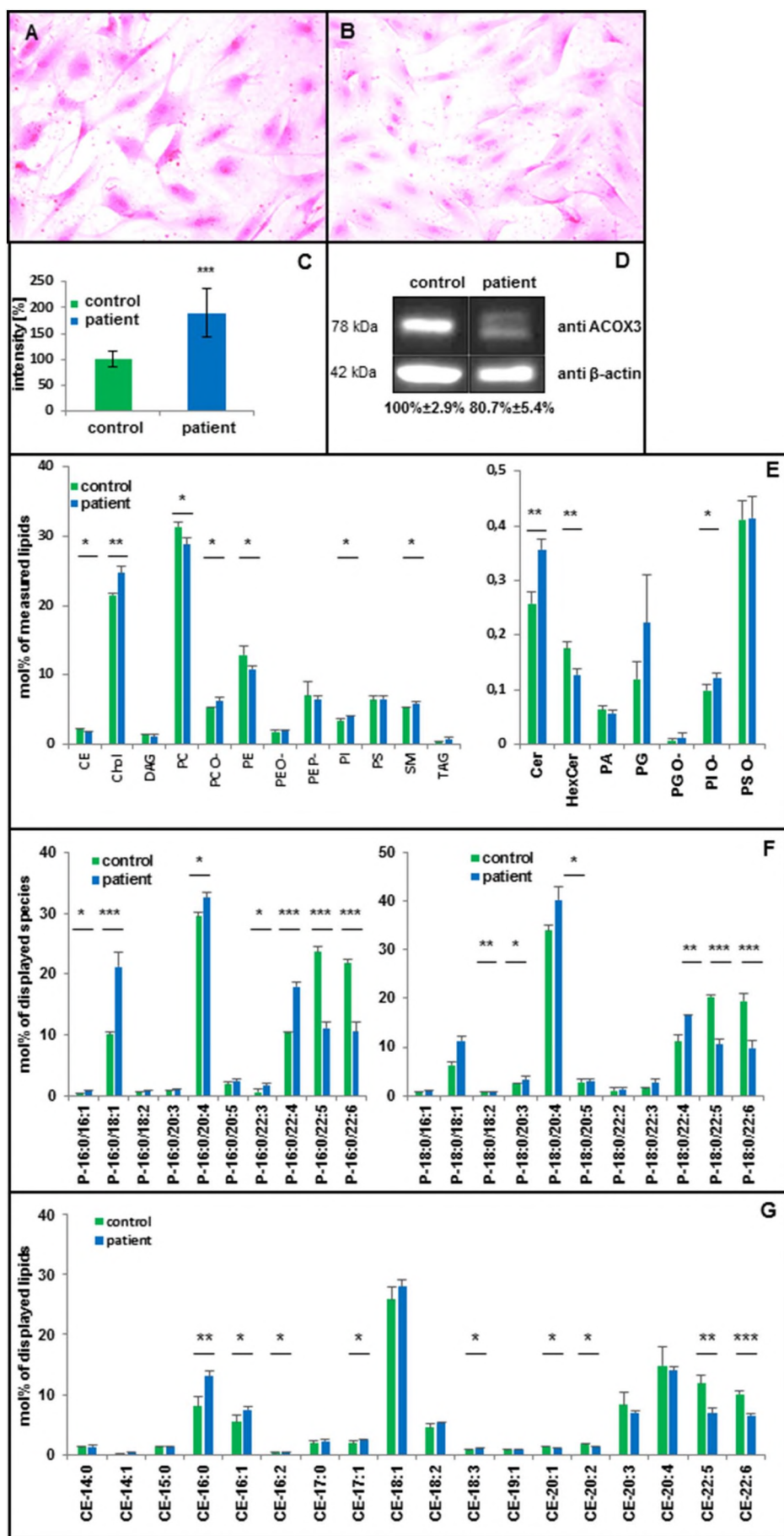
Fig. 5. Analysis of the cellular lipid homeostasis and ACOX3 expression. Staining of lipids in control (A) and patient fibroblasts (B) with Oil Red O after stressing with CuSO$_4$ showed a more pronounced coloration in case of the ATP6AP1-CDG patient. (C) Quantification of the staining intensity in control and patient-derived fibroblasts. (D) Peroxisomal function was assessed by Western blotting with an antibody against ACOX3 which showed a diminished signal in case of the patient. (E) Nano-electrospray ionization tandem mass spectrometry of cellular lipids showed alterations in the main lipid classes. While phosphatidylcholine (PC) and phosphatidylethanolamine (PE) were decreased, cholesterol (Chol) was enriched in the patient's fibroblasts (left part). Within the minor lipid species, hexosyl ceramide (HexCer) was significantly reduced, while ceramide (Cer) was significantly increased (right part). (F) As to the plasmalogens (P-16:0 and P-18:0) elevated levels of 18:1, 20:4 and 22:4 species and reduced amounts of 22:5–22:6 species were present in the patient. (G) Measurement of cholesteryl esters (CE-14:0 to CE-22:6) revealed a broad lipid dysregulation. Lipid abbreviations are mentioned below.

of cellular lipids revealed some minor but significant alterations within the main lipid classes (Supp. Table 2). At the expense of phosphatidylcholine (PC; 28.8 mol% ± 1.0 mol%, *p ≤ 0.009) and phosphatidylethanolamine (PE; 10.9 mol% ± 0.5 mol%, *p ≤ 0.03), cholesterol (Chol) was slightly enriched in the patient's fibroblasts (24.7 mol% ± 0.9 mol%, **p ≤ 0.002) in contrast to the control (PC, 31.4 mol% ± 0.6 mol%; PE, 12.9 mol% ± 1.3 mol%; Chol, 21.5 mol% ± 0.2 mol%). Within the minor lipid species, hexosyl ceramide (HexCer; 0.13 mol% ± 0.01 mol%, **p ≤ 0,003) was significantly reduced, while its immediate precursor ceramide (Cer; 0.36 mol% ± 0.02 mol%, **p ≤ 0.002) was significantly increased (0.18 mol% ± 0.01 mol% HexCer; 0.26 mol% ± 0.02 mol% Cer) (Fig. 5, E). In addition, abnormalities of the plasmalogens (16:0 and 18:0) were detected, indicated by significantly elevated levels of 18:1, 20:4 and 22:4 species in combination with significantly reduced amounts of 22:5 and 22:6 species (Fig. 5, F). Besides, allocation of cholesteryl esters (CE) was impacted as well, designated by several significantly deregulated metabolites between CE-16:0 and CE-22:6 (Fig. 5, G). From CE-16:0 to CE-19:1 we found an increase of lipids in the patient samples whereas lipid species from CE-20:1 to CE-22:6 were decreased (Suppl. Table 2). Similar effects were seen for the PE lipid class and phosphatidylserine (data not shown).

3.9. Reduced ACOX3 expression and diminished catalase activity point to dysregulation of the peroxisomal ß-oxidation

Finally we focused on the peroxisomal ß-oxidation. The expression of ACOX3 was significantly reduced in patient fibroblasts (80.7% ± 5.4%, ***p ≤ 0.003; control 100% ± 2.9%; Fig. 5, D). Moreover, catalase activity was significantly diminished with a residual activity of 0.72 nmol/min/ml (63.02% ± 0.08%; control, 1.14 nmol/min/ml, 100% ± 0.03%). Both results indicate an effect on peroxisomal function.

4. Discussion

Deficiencies in several subunits of the V-ATPase multi-subunit complex lead to hypoglycosylation of proteins and subsequently to different CDG types. Here we describe a patient with a hemizygous mutation in ATP6AP1, one of the accessory subunits of the vacuolar H$^+$-ATPase (V-ATPase).

Although no neurocognitive deficits, epilepsy, signs of hearing loss or ocular impairment were noted, our patient presents several features found in the recently reported 11 ATP6AP1-CDG patients as liver and spleen involvement, low amount of immunoglobulins and bad outcome after vaccinations [14] (OMIM: 300197). Concerning the patient's immunological deficits, it is interesting to note the detected low level of ceruloplasmin, the main transport protein of copper in blood. As it normally binds > 90% of the total copper amount [24], its reduction can subsequently lead to copper shortage. Next to zinc and iron, copper displays the third most important essential trace element in men in fulfilling broad tasks e.g. as cofactor for several enzymes, in hematopoiesis and by supporting the immune system [25,26,27]. A connection between X-linked cutis laxa and a copper-dependent enzyme displays the lysyl oxidase which is necessary to cross-link collagen and elastin in the extracellular matrix [28,29]. In addition to the dermal phenotype patients also showed reduced copper and ceruloplasmin [30,31]. Besides, acquired cutis laxa can be caused by administration of copper chelators as penicillamine which was shown in patients with Wilson's Disease [32]. Interestingly, the skin phenotype of our patient mostly regressed within the next 14 months. This has also been observed in other CDG caused by defects in alternative subunits of the V-ATPase complex: ATP6V0A2, ATP6V1A and ATP6V1E1 [7,33]. Currently, the clinical presentation of the different V-ATPase deficiencies shows distinct variances, which could support the identification of the underlying defect of new CDG-II patients with cutis laxa. In ATP6V0A2-CDG the

cutis laxa symptoms improve and there is no brain involvement, comparable to ATP6AP1-CDG. But in ATP6V0A2-CDG the mainly affected organs are eyes, neuromuscular system and skeleton [34,35], not liver or spleen. In ATP6V1A-CDG cutis laxa also declines but cardiac involvement and neurological symptoms as epilepsy and speech disability dominate. Consistent with ATP6AP1-CDG, in ATP6V1E1-CDG no neurological involvement is detected but cutis laxa does not improve [7]. However, due to the small number of known V-ATPase deficient patients, this clinical spectrum is still evolving.

In addition exocrine pancreatic insufficiency was detected, which presumably resulted in diarrhea, growth retardation and a reduced absorbance of the fat-soluble vitamins A, D, E and K. Vitamin A deficiency causes dryness and keratinization in epithelial cells of the skin, the respiratory, gastrointestinal and urogenital tracts, all of which are initial preventative systems against infections. These disruptions can lead to a general decrease in the body's ability to eliminate infections [36,37,38]. Low levels of vitamin D, E and K have been observed in patients with respiratory infections and general problems in immune response. Vitamin D is also important for skin health, regeneration, function and elasticity [39,40,41,42,43]. The lack of vitamins together with a potential reduced lysyl oxidase activity could have contributed to the skin phenotype and higher infection rate of the patient in infancy before oral vitamin supplementation.

Although the physical and cognitive progression of our patient is very satisfying (2018), the glycosylation defect is still present albeit in a less pronounced status than in his first year (2008). The investigation of the patient's N-glycans by mass spectrometry showed in particular diantennary structures with loss of N-acetylglucosamine, galactose and sialic acid residues in parallel to an overall reduction of complex sialylated structures. A comparable result is also reflected in patients suffering from the other V-ATPase defects [7,14,33] and hints to a broad pH-dependent mismanagement of Golgi glycosyltransferases. Notably, a pronounced accumulation of Man$_5$GlcNAc$_2$ (H5N2) was present. Since the flow into the direction of complex-type moieties is diminished, one could speculate that H5N2 emerged due to a potential feedback at the level of the medial Golgi GlcNAc transferase MGAT1 which controls the synthesis of hybrid and complex-type N-glycans [44]. Since we did not only detect a shift towards more hybrid structures (~ plus 80%) but also a prominent shift to mannose-rich structures (~ plus 90%) on proteins, a diversion to these alternative N-glycan pathways can be assumed.

The new mutation in the ATP6AP1 gene c.542 T > G (p.L181R) concerns a highly conserved amino acid within species. Quantitative RT-PCR studies revealed that the decrease of the ATP6AP1 protein quantity (~ 49%) detected by Western blot and immunofluorescence analyses was due to a decreased mRNA amount (~ 57%). We did not further address if either reduced ATP6AP1-mRNA synthesis or mRNA instability were causal.

The biochemical impact of the mutated ATP6AP1 results in a significantly elongated doubling time and reduced proliferation of the patient's fibroblasts. We could exclude apoptosis as a cause. ER stress was slightly elevated and levels of several amino acids were borderline and some even reduced. Both could affect cell viability [45,46]. In fibroblasts, we also detected an altered acylcarnitine and lipid homeostasis mostly marked by a significant increase of the saturated, very long-chain, branched pristanic and phytanic fatty acids as well as by diminished amounts of phosphatidylcholine and phosphatidylethanolamine, whereas cholesterol and ceramide were elevated. Abnormalities of the plasmalogens, phosphatidylserine and the cholesteryl esters were also observed and pointed to a defect in the peroxisomal ß-oxidation. This was further confirmed by a significantly diminished ACOX3 expression and a significantly reduced catalase activity. Nevertheless, its mechanism remains to be elucidated.

5. Conclusion

In conclusion, we could show that deficiency of the accessory subunit ATP6AP1 of the V-ATPase leads to a broad spectrum of abnormalities characterized by shortening of protein bound N-glycans in serum and dysregulation of the amino acids as well as lipid homeostasis in fibroblasts. We hereby extend the knowledge on this rare type of CDG, which will help to understand its phenotype, in particular the cutis laxa, immunological and liver abnormalities.

Conflict of interest

The authors have no conflict of interest to declare.

Appendix A. Supplementary data

Supplementary data to this article can be found online at https://doi.org/10.1016/j.ymgme.2018.01.008.

References

[1] I.H. Madshus, Regulation of intracellular pH in eukaryotic cells, Biochem. J. 250 (1988) 1–8.

[2] J.R. Casey, S. Grinstein, J. Orlowski, Sensors and regulators of intracellular pH, Nat. Rev. Mol. Cell Biol. 11 (2010) 50–61.

[3] V. Marshansky, J.L. Rubinstein, G. Grüber, Eukaryotic V-ATPase: novel structural findings and functional insights, Biochim. Biophys. Acta 1837 (2014) 857–879.

[4] M.E. Finbow, M.A. Harrison, The vacuolar H + -ATPase: a universal proton pump of eukaryotes, Biochem. J. 324 (1997) 697–712.

[5] K. Cotter, L. Stransky, C. McGuire, M. Forgac, Recent insights into the structure, regulation, and function of the V-ATPases, Trends Biochem. Sci. 40 (2015) 611–622.

[6] D. Batlle, S.K. Haque, Genetic causes and mechanisms of distal renal tubular acidosis, Nephrol. Dial. Transplant. 27 (2012) 3691–3704.

[7] T. Van Damme, T. Gardeitchik, M. Mohamed, S. Guerrero-Castillo, P. Freisinger, B. Guillemyn, A. Kariminejad, D. Dalloyaux, S. Van Kraaij, D.J. Lefeber, D. Syx, W. Steyaert, R. De Rycke, A. Hoischen, E.J. Kamsteeg, S.Y. Wong, M. Van Scherpenzeel, P. Jamali, U. Brandt, L. Nijtmans, G.C. Korenke, B.H.Y. Chung, C.C.Y. Mak, I. Hausser, U. Kornak, B. Fischer-Zirnsak, T.M. Strom, T. Meitinger, Y. Alanay, G.E. Utine, P.K.C. Leung, S. Ghaderi-Sohi, P. Coucke, S. Symoens, A. De Paepe, C. Thiel, T.B. Haack, F. Malfait, E. Morava, B. Callewaert, R.A. Wevers, Mutations in ATP6V1E1 or ATP6V1A cause autosomal-recessive cutis laxa, Am. J. Hum. Genet. 100 (2017) 216–227.

[8] U. Kornak, A. Schulz, W. Friedrich, S. Uhlhaas, B. Kremens, T. Voit, C. Hasan, U. Bode, T.J. Jentsch, C. Kubisch, Mutations in the a3 subunit of the vacuolar H (+)-ATPase cause infantile malignant osteopetrosis, Hum. Mol. Genet. 9 (2000) 2059–2063.

[9] A. Frattini, P.J. Orchard, C. Sobacchi, S. Giliani, M. Abinun, J.P. Mattsson, D.J. Keeling, A.K. Andersson, P. Wallbrandt, L. Zecca, L.D. Notarangelo, P. Vezzoni, A. Villa, Defects in TCIRG1 subunit of the vacuolar proton pump are responsible for a subset of human autosomal recessive osteopetrosis, Nat. Genet. 25 (2000) 343–346.

[10] K.J. Borthwick, F.E. Karet, Inherited disorders of the H + -ATPase, Curr. Opin. Nephrol. Hypertens. 11 (2002) 563–568.

[11] H.V. Gupta, J. Vengoechea, K. Sahaya, T. Virmani, A splice site mutation in ATP6AP2 causes X-linked intellectual disability, epilepsy, and parkinsonism, Parkinsonism Relat. Disord. 21 (2015) 1473–1475.

[12] J. Jaeken, R. Péanne, What is new in CDG? J. Inherit. Metab. Dis. 40 (2017) 569–586.

[13] U. Kornak, E. Reynders, A. Dimopoulou, J. Van Reeuwijk, B. Fischer, A. Rajab, B. Budde, P. Nürnberg, F. Foulquier, ARCL Debré-type Study Group, D. Lefeber, Z. Urban, S. Gruenewald, W. Annaert, H.G. Brunner, H. Van Bokhoven, R. Wevers, E. Morava, G. Matthijs, L. Van Maldergem, S. Mundlos, Impaired glycosylation and cutis laxa caused by mutations in the vesicular H + -ATPase subunit ATP6V0A2, Nat. Genet. 40 (2008) 32–34.

[14] E.J. Jansen, S. Timal, M. Ryan, A. Ashikov, M. Van Scherpenzeel, L.A. Graham, H. Mandel, A. Hoischen, T.C. Iancu, K. Raymond, G. Steenbergen, C. Gilissen, K. Huijben, N.H. Van Bakel, Y. Maeda, R.J. Rodenburg, M. Adamowicz, E. Crushell, H. Koenen, D. Adams, J. Vodopiutz, S. Greber-Platzer, T. Müller, G. Dueckers, E. Morava, J. Sykut-Cegielska, G.J. Martens, R.A. Wevers, T. Niehues, M.A. Huynen, J.A. Veltman, T.H. Stevens, D.J. Lefeber, ATP6AP1 deficiency causes an immunodeficiency with hepatopathy, cognitive impairment and abnormal protein glycosylation, Nat. Commun. 7 (2016) 11600.

[15] R. Niehues, M. Hasilik, G. Alton, C. Körner, M. Schiebe-Sukumar, H.G. Koch, K.P. Zimmer, R. Wu, E. Harms, K. Reiter, K. Von Figura, H.H. Freeze, H.K. Harms, T. Marquardt, Carbohydrate-deficient glycoprotein syndrome type 1b. Phosphomannose isomerase deficiency and mannose therapy, J. Clin. Invest. 101 (1998) 1414–1420.

[16] S. Wopereis, S. Grünewald, E. Morava, J.M. Penzien, P. Briones, M.T. García-Silva, P.N. Demacker, K.M. Huijben, R.A. Wevers, Apolipoprotein C-III isofocusing in the diagnosis of genetic defects in O-glycan biosynthesis, Clin. Chem. 49 (2003) 1839–1845.

[17] J. Lübbehusen, C. Thiel, N. Rind, D. Ungar, B.H. Prinsen, T.J. De Koning, P.M. Van Hasselt, C. Körner, Fatal outcome due to deficiency of subunit 6 of the conserved oligomeric Golgi complex leading to a new type of congenital disorders of glycosylation, Hum. Mol. Genet. 19 (2010) 3623–3633.

[18] K.R. Reiding, D. Blank, D.M. Kuijper, A.M. Deelder, M. Wuhrer, High-throughput profiling of protein N-glycosylation by MALDI-TOF-MS employing linkage-specific sialic acid esterification, Anal. Chem. 86 (2014) 5784–5793.

[19] C. Evers, C. Staufner, M. Granzow, N. Paramasivam, K. Hinderhofer, L. Kaufmann, C. Fischer, C. Thiel, T. Opladen, U. Kotzaeridou, S. Wiemann, M. Schlesner, R. Eils, S. Kölker, C.R. Bartram, G.F. Hoffmann, U. Moog, Impact of clinical exomes in neurodevelopmental and neurometabolic disorders, Mol. Genet. Metab. 121 (2017) 297–307.

[20] B. Hansske, C. Thiel, T. Lübke, M. Hasilik, S. Höning, V. Peters, P.H. Heidemann, G.F. Hoffmann, E.G. Berger, K. Von Figura, C. Körner, Deficiency of UDP-galactose: N-acetylglucosamine beta-1,4-galactosyltransferase I causes the congenital disorder of glycosylation type II, J. Clin. Invest. 109 (2002) 725–733.

[21] J.G. Okun, S. Conway, K.V. Schmidt, J. Schumacher, X. Wang, R. De Guia, A. Zota, J. Klement, O. Seibert, A. Peters, A. Maida, S. Herzig, A.J. Rose, Molecular regulation of urea cycle function by the liver glucocorticoid receptor, Mol. Metab. 4 (2015) 732–740.

[22] H. Ahlgren, C. Bas-Orth, H.E. Freitag, A. Hellwig, O.P. Ottersen, H. Bading, The nuclear calcium signaling target, activating transcription factor 3 (ATF3), protects against dendrotoxicity and facilitates the recovery of synaptic transmission after an excitotoxic insult, J. Biol.Chem. 289 (2014) 9970–9982.

[23] C. Özbalci, T. Sachsenheimer, B. Brügger, Quantitative analysis of cellular lipids by nano-electrospray ionization mass spectrometry, Methods Mol. Biol. 1033 (2013) 3–20.

[24] N.E. Hellman, J.D. Gitlin, Ceruloplasmin: metabolism and function, Annu. Rev. Nutr. 22 (2002) 439–458.

[25] W. Nijhof, M. Holtrop, J. De Jonge, H. Hartsuiker, H. De Vries, Severe reductions in transcripts for cytochrome c oxidase during erythropoiesis in vitro do not lead to inactive mitochondria in reticulocytes, Exp. Hematol. 19 (1991) 359–363.

[26] R.I. Bustos, E.L. Jensen, L.M. Ruiz, S. Rivera, S. Ruiz, F. Simon, C. Riedel, D. Ferrick, A.A. Elorza, Copper deficiency alters cell bioenergetics and induces mitochondrial fusion through up-regulation of MFN2 and OPA1 in erythropoietic cells, Biochem. Biophys. Res. Commun. 437 (2013) 426–432.

[27] T.N. Tarasenko, S.E. Pacheco, M.K. Koenig, J. Gomez-Rodriguez, S.M. Kapnick, F. Diaz, P.M. Zerfas, E. Barca, J. Sudderth, R.J. DeBerardinis, R. Covian, R.S. Balaban, S. DiMauro, P.J. McGuire, Cytochrome c oxidase activity is a metabolic checkpoint that regulates cell fate decisions during T cell activation and differentiation, Cell Metab. 25 (2017) 1254–1268.

[28] L.I. Smith-Mungo, H.M. Kagan, Lysyl oxidase: properties, regulation and multiple functions in biology, Matrix Biol. 16 (1998) 387–398.

[29] A. Khakoo, R. Thomas, R. Trompeter, P. Duffy, R. Price, F.M. Pope, Congenital cutis laxa and lysyl oxidase deficiency, Clin. Genet. 51 (1997) 109–114.

[30] H. Kodama, C. Fujisawa, W. Bhadhprasit Curr Drug Metab, Inherited Copper Transport Disorders: Biochemical Mechanisms, Diagnosis, and Treatment, 13 (2012), pp. 237–250.

[31] Z. Urban, E.C. Davis, Cutis laxa: intersection of elastic fiber biogenesis, TGFβ signaling, the secretory pathway and metabolism, Matrix Biol. 33 (2014) 16–22.

[32] V.A. Hill, C.A. Seymour, P.S. Mortimer, Pencillamine-induced elastosis perforans serpiginosa and cutis laxa in Wilson's disease, Br. J. Dermatol. 142 (2000) 560–561.

[33] L. Van Maldergem, W. Dobyns, U. Korna, ATP6V0A2-Related Cutis Laxa, in: R.A. Pagon, M.P. Adam, H.H. Ardinger, S.E. Wallace, A. Amemiya, L.J.H. Bean, T.D. Bird, N. Ledbetter, H.C. Mefford, R.J.H. Smith, K. Stephens (Eds.), GeneReviews® [Internet]. Seattle (WA), University of Washington, Seattle, 2009.

[34] M. Mohamed, M. Guillard, S.B. Wortmann, S. Cirak, E. Marklova, H. Michelakakis,

E. Korsch, M. Adamowicz, B. Koletzko, F.J. Van Spronsen, K.E. Niezen-Koning, G. Matthijs, T. Gardeitchik, D. Kouwenberg, B.C. Lim, R. Zeevaert, R.A. Wevers, D.J. Lefeber, E. Morava, Clinical and diagnostic approach in unsolved CDG patients with a type 2 transferrin pattern, Biochim. Biophys. Acta 1812 (2011) 691–698.

[35] D. Bahena-Bahena, J. López-Valdez, K. Raymond, R. Salinas-Marín, A. Ortega-García, B.G. Ng, H.H. Freeze, M. Ruíz-García, I. Martínez-Duncker, ATP6V0A2 mutations present in two Mexican Mestizo children with an autosomal recessive cutis laxa syndrome type IIA, Mol. Genet. Metab. Rep. 1 (2014) 203–212.

[36] C.B. Stephensen, Vitamin A, infection, and immune function, Annu. Rev. Nutr. 21 (2001) 167–192.

[37] A. Barua, M. Stacewicz-Sapuntzakis, H. Furr, Vitamin A - retinol, in: W. Herrmann, R. Obeid (Eds.), Vitamins in the Prevention of Human Diseases, Walter de Gruyter, New York, 2011, pp. 7–39.

[38] W. Chen, G. Chen, The roles of vitamin A in the regulation of carbohydrate, lipid, and protein metabolism, J. Clin. Med. 3 (2014) 453–479.

[39] M.F. Holick, Sunlight and vitamin D for bone health and prevention of autoimmune diseases, cancers, and cardiovascular disease, Am. J. Clin. Nutr. 80 (2004) 1678S–1688S.

[40] M.W. Clarke, J.R. Burnett, K.D. Croft, Vitamin E in human health and disease, Crit. Rev. Clin. Lab. Sci. 45 (2008) 417–450.

[41] L.A. Plum, H.F. DeLuca, Vitamin D, disease and therapeutic opportunities, Nat. Rev. Drug Discov. 9 (2010) 941–955.

[42] J.A. Beard, A. Bearden, R. Striker, Vitamin D and the anti-viral state, J. Clin. Virol. 50 (2011) 194–200.

[43] A.A. Albahrani, R.F. Greaves, Fat-soluble vitamins: clinical indications and current challenges for chromatographic measurement, Clin. Biochem. Rev. 37 (2016) 27–47.

[44] B. Yip, S.H. Chen, H. Mulder, J.W. Höppener, H. Schachter, Organization of the human beta-1,2-N-acetylglucosaminyltransferase I gene (MGAT1), which controls complex and hybrid N-glycan synthesis, Biochem. J. 321 (1997) 465–474.

[45] A. Suraweera, C. Münch, A. Hanssum, A. Bertolotti, Failure of amino acid home-ostasis causes cell death following proteasome inhibition, Mol. Cell 48 (2012) 242–253.

[46] L. Matos, A.M. Gouveia, H. Almeida, ER stress response in human cellular models of senescence, J. Gerontol. A. Biol. Sc. Med. Sci. 70 (2015) 924–935.